THE EFFECT OF HEAT INPUT ON MICROSTRUCTURE AND CRACKING IN ALLOY 625 WELD OVERLAYS

I.L.W. Wilson, R.G. Gourley, R.M. Walkosak, and G.J. Bruck*

Westinghouse Electric Corporation
Electro-Mechanical Division
Cheswick Avenue
Cheswick, Pennsylvania 15024

Abstract

Weld overlays of alloy 625 have been deposited on AISI Type 304 stainless steel using PTA, GTAW and laser welding processes. Cracking was observed in the weld deposited overlay with higher heat input. The lower heat inputs resulted in sound weld overlays. The cracking was found to be associated with second phase particles in the weldment. Metallography and scanning electron microscopy with EDXA were used to analyze the particles. Particle analyses and morphological characteristics revealed the presence of Laves phase. The size and distribution of this phase is affected by the heat input during welding and can be controlled to avoid problems with cracking.

* Westinghouse Science & Technology Center
1310 Beulah Road
Pittsburgh, Pennsylvania 15235

Superalloys 718, 625 and Various Derivatives
Edited by Edward A. Loria
The Minerals, Metals & Materials Society, 1991

Introduction

Inconel 625 is a corrosion resistant nickel base alloy used extensively for its wear resistance in aggressive, chloride bearing, environments. Wrought, cast, powder metallurgy and weld overlay products have been used. Alloy 625 has also demonstrated excellent performance in nuclear power plant operation environments (Ref. 1) where the operating chemistries are less aggressive but where very reliable long-term performance is required. For this reason, the alloy has been investigated for applications in the reactor system. The purpose of the present investigation is to develop a method for producing reliable, defect-free weld overlays of alloy 625 on AISI Type 304 stainless steel using production welding techniques. During the initial trials, cracking was observed in the overlay. Metallographic examination revealed that the cracking was associated with second phase particles which were identified as Laves phase, (Refs. 2,3,4). This paper reports the investigation of the occurrence of Laves phase in alloy 625 weld overlays using three production welding processes with varying heat inputs.

Experimental

Three weld processes were used to deposit Inconel 625 onto AISI 304 stainless steel. These processes were plasma transferred arc (PTA), gas tungsten arc welding with automatic cold wire feed (GTAW) and laser cladding. These processes were selected because they represented significant variations of welding heat input, the key process variable.

The PTA process employed Nistelle 625 powder, mesh 100/325 and an AISI 304 stainless substate. The equipment used was a Linde PSM-2 Surface Welder with a PT 9 torch. The AISI 304 base material was a ring measuring 2.0 inches thick, with an outside diameter of 10.9 inch and an inside diameter of 9.3 inch. The weld overlay was placed on one face of the ring. The welding was conducted in two layers of 0.1 inch thickness in the root and 0.125 inch thickness in the second layer. Prior to welding the second layer, the first layer was machined to remove any surface oxidation. The second layer was machined to generate a smooth surface and penetrant testing was performed to verify soundness of the weld.

The GTAW process was used with 0.045 inch diameter ERNiCrMo-3 filler wire; its chemistry is given in Table 1. The equipment used was a Miller power source with a Linde wire drive unit and an automatic voltage control (AVC) head with a HW27 torch.

The AISI 304 stainless steel base material was a ring measuring 2.2 inches thick with an outside diameter of 10.5 inch and an inside diameter of 8.5 inch. The weld overlay was deposited on one of the two faces of the ring. The first layer was welded followed by interpass/bead grinding and a penetrant test of the root layer. The thickness of the root layer was 0.08 inch. The second layer was deposited creating a build-up of 0.115 inch, and it also was ground and penetrant tested. The weld parameters are defined in Table 2. Eight weld beads were deposited in the root layer and 7 were required for the second layer. The weld beads were deposited starting from the inside diameter and working outward toward the outside diameter.

Table 1: Chemistry of Inconel Powder and Wire

	C	Cr	Fe	Mn	Mo	Ni	P	S	Si	Cb.Ta	Al	Ti
Nistelle 625 Powder	0.05	22.17	2.30	0.40	9.22	61.1	.005	.002	.39	3.71	0.19	.29
.045 Dia. Inconel 625 Wire	0.05	22.04	3.75	0.15	9.16	60.86	.008	<.001	0.11	3.48	0.13	.26

Table 2: Weld Process Parameters and Heat Input (KJ/in^2)

	PTA	GTAW	Laser
Power Source	DC	DC	--
Polarity	DCSP	DCSP	--
Amps	165	70	--
Volts	30	12	--
Travel Speed	2.25 IPM	2 IPM	8 IPM
Wire Feed Speed	--	93 IPM	--
Max. Interpass Temp.	350° F	150° F	--
Oscillation Width	0.750 - 1.0"	--	--
Oscillation Speed	24-32 OPM	--	--
Scan Amplitude	--	--	0.75"
Scan Frequency	--	--	15 Hz
Powder Depth	--	--	0.075"
Pass Overlap	--	--	0.375"
Atmosphere	--	--	Argon
Delivered Power	--	--	5.6 KW
Shield Gas and Flow	75% He 25% Ar (50 CFH)	Argon (45 CFH)	--
Bead Width	1.0"	0.375"	0.750"
No. of Beads	1	7-8	1
Heat Input	132 (KJ/in^2)	67 (KJ/in^2)	56 (KJ/in^2)

Note:
IPM = Inches Per Minute
OPM = Oscillations Per Minute
DCSP = Direct Current Straight Polarity

The laser cladded samples were produced using an Avco HPL continuous wave carbon dioxide laser rated at 15 kilowatts output power. Nistelle 625 powder was preplaced on the 304 substrate and the laser beam was used to melt the preplace and fuse it with the substrate. Each pass was positioned with a 0.375 inch overlap of the preceding pass. Two complete layers were applied. The 304 stainless steel sample was in an unrestrained position, in a controlled atmosphere chamber and oriented such that its major axis was parallel to the direction of carriage motion. A narrow slot in the chamber cover permitted laser beam access. Pure argon purge gas was supplied through a manifold system enclosed in a plenum beneath the porous metal base of the chamber. An oxygen monitor was used to confirm that shielding was adequate in preventing contamination during processing. After welding each pass, light grinding was applied to remove oxidation prior to depositing the next pass. Subsequent passes were also ground and finally, the entire layer was ground 0.020 inch to remove any surface irregularities and oxidation. The process parameters used are illustrated in Table 2. This procedure and aforementioned precautions regarding shielding are routine, recommended practices for laser beam cladding. The size of the plate clad was 1.0 inch x 6.0 inch x 54.0 inch. The Chemistry of the Nistelle 625 powder can be found in Table 1. Its mesh size was 100/325.

All welded samples were cross-sectioned, mounted and metallographically prepared for examination using standard light microscopy and a Amray model 1645 scanning electron microscope fitted with Kevex series 82 Energy Dispersive X-ray Analysis (EDXA) system. The spot size used for analysis was 1/2 micrometers. The etchant used for all specimens was a 6% solution of chromic acid in water.

Results and Discussion

The initial attempt at applying an alloy 625 weld overlay was conducted using the PTA technique. Cracking was revealed by penetrant testing of the surface after machining. Cross-sections showed that the cracking was present in the overlay down to the 304 stainless steel substrate; see Figs. 1, 2, and 3. The cracking was associated with the concentration of second phase particles in the microstructure, (Fig. 3). EDXA analyses of these particles revealed increased levels of Nb, Mo, and Si compared to the concentrations in the overlay matrix; see Table 3. This segregation is typical of that found in such highly allowed welded materials and has been identified as Laves phase (Ref. 5). The composition of the alloy 625 powder, Table 1, shows Nb, Mo, and Si to be sufficiently high such that it would result in Laves phase formation (Ref. 5).

Although the carbon content is high, no indications of carbide precipitates were observed. The EDXA analyses were close to the 304 stainless steel interface which accounts for the high Fe content in the weld overlay.

Fig. 1: Photomicrograph through Cross-Section of Plasma Transferred Arc (PTA) Weldment.
Magnification 200X

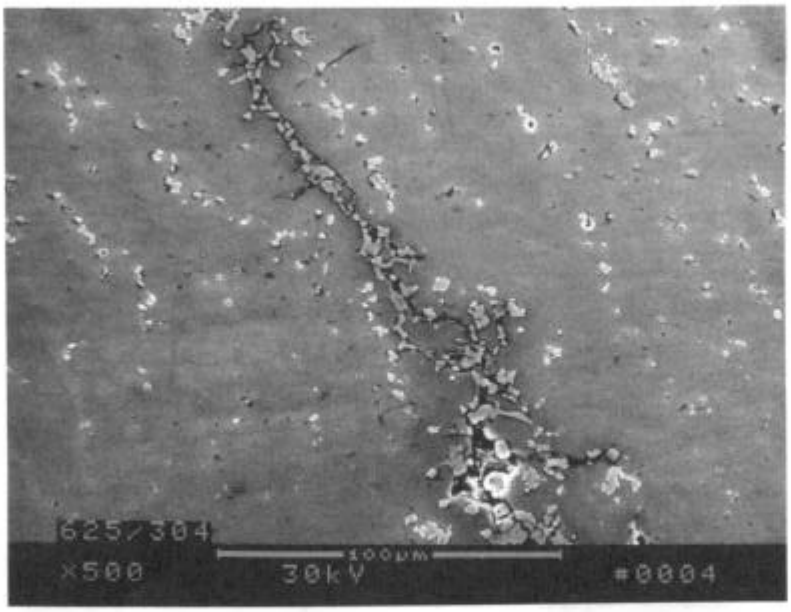

Fig. 2: Scanning Electron Micrograph of PTA Weldment Cross-Section. Magnification 500X

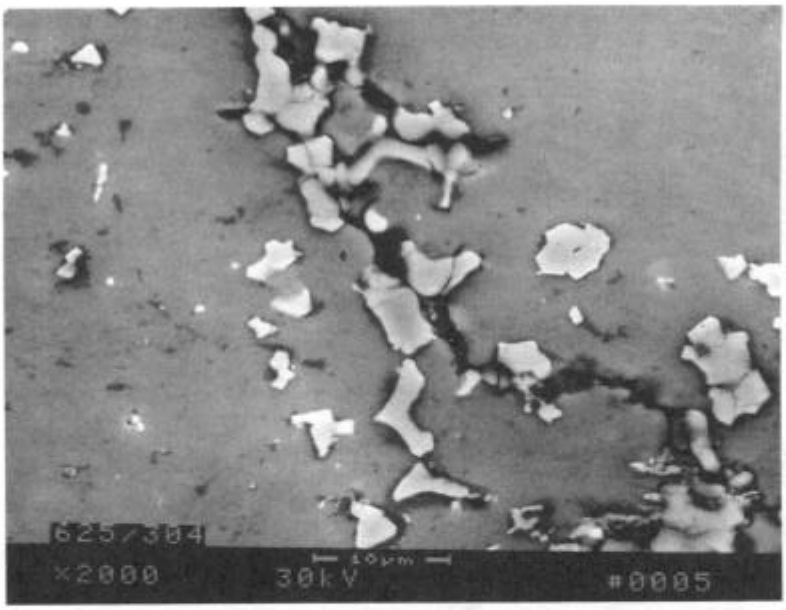

Fig. 3: Scanning Electron Micrograph of PTA Weldment Cross-Section. Magnification 2000X

Table 3: EDXA Analysis of Weldments

	Wt %					
Specimen	Nb	Mo	Si	Cr	Fe	Ni
PTA Particle	27.51	17.10	9.69	12.46	12.92	20.31
PTA Matrix	3.73	8.08	2.25	21.40	27.51	37.03
GTAW Particle	13.40	13.58	6.12	18.35	8.02	40.54
GTAW Matrix	4.89	9.47	3.93	21.76	9.57	50.38
Laser Particle	12.26	18.57	8.23	17.35	6.89	36.70
Laser Matrix	4.27	9.84	4.82	21.99	7.42	51.67

No cracking was observed in the GTAW weld overlay; see Figs. 4 and 5. The composition of the wire consumable is again relatively high for Si, Mo, and Nb, indicating that Laves phase could be readily formed. It can be seen from the cross-section through the overlay, Figs. 4 and 5, that the size of the second phase particles is smaller than was observed in the PTA overlay. The EDXA analyses from the particles, Table 3, shows less segregation compared to the PTA overlay.

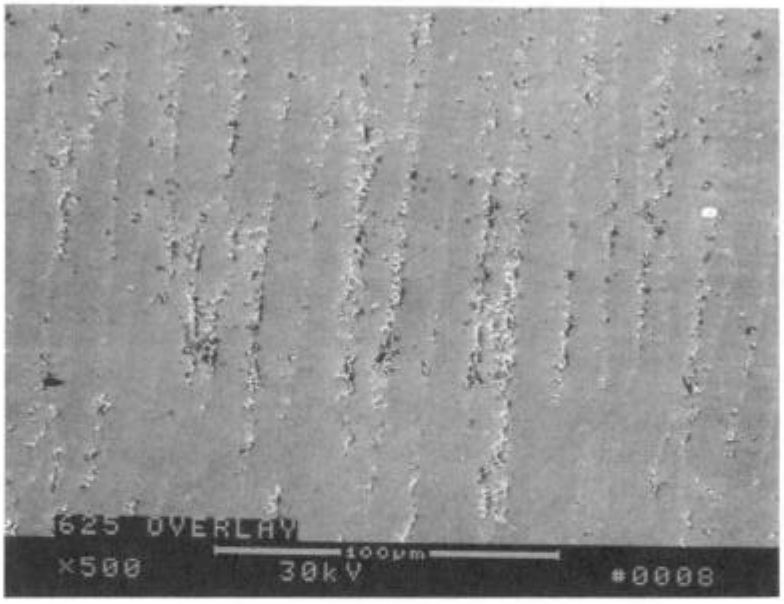

Fig. 4: Photo Micrograph through Cross-Section of Gas Tungsten Arc (GTAW) Weldment
Magnification 500X

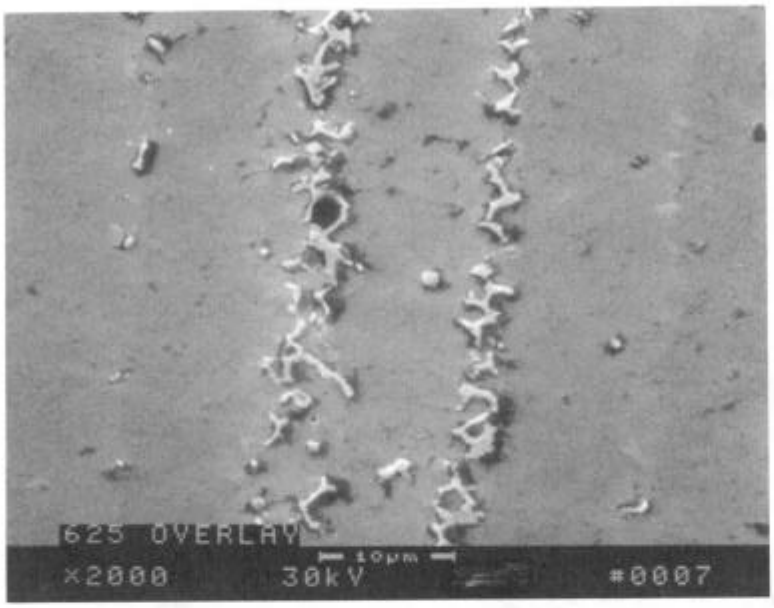

Fig. 5: Scanning Electron Micrograph of GTAW Cross-Section. Magnification 2000X

The appearance of the laser weld overlay, using powder, is very similar to the GTAW weld overlay using wire. The second phase particles are somewhat finer and more evenly distributed; see Figs. 6 and 7. The segregation of Si, Mo and Nb into the particles is similar to that found in the GTAW weld; see Table 3. Some segregation within the matrix is present, as indicated by the light area of the matrix adjacent to the particles in the back-scattered SEM photomicrographs of Figs. 6 and 7. Examples of the EDXA spectra from the Laves phase particles and the matrix are shown in Figs. 8A and 8B.

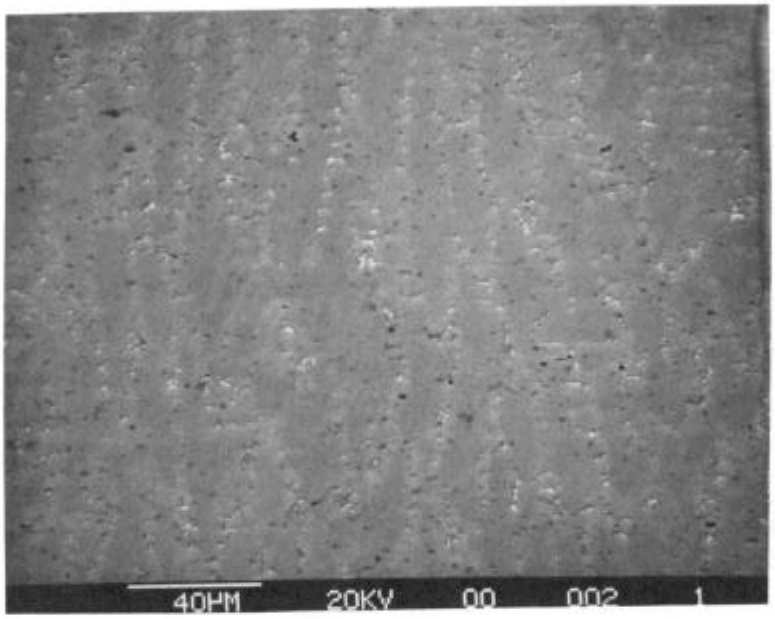

Fig. 6: Scanning Electron Micrograph of Laser Cross-Section (Back-Scatter Mode).
Magnification 500X

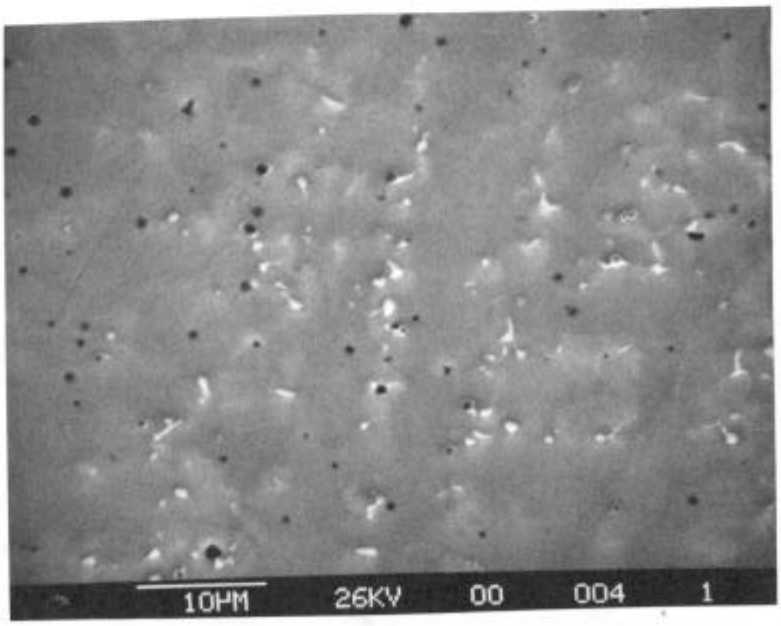

Fig. 7: Scanning Electron Micrograph of Laser Cross-Section (Back-Scatter Mode).
Magnification 2000X

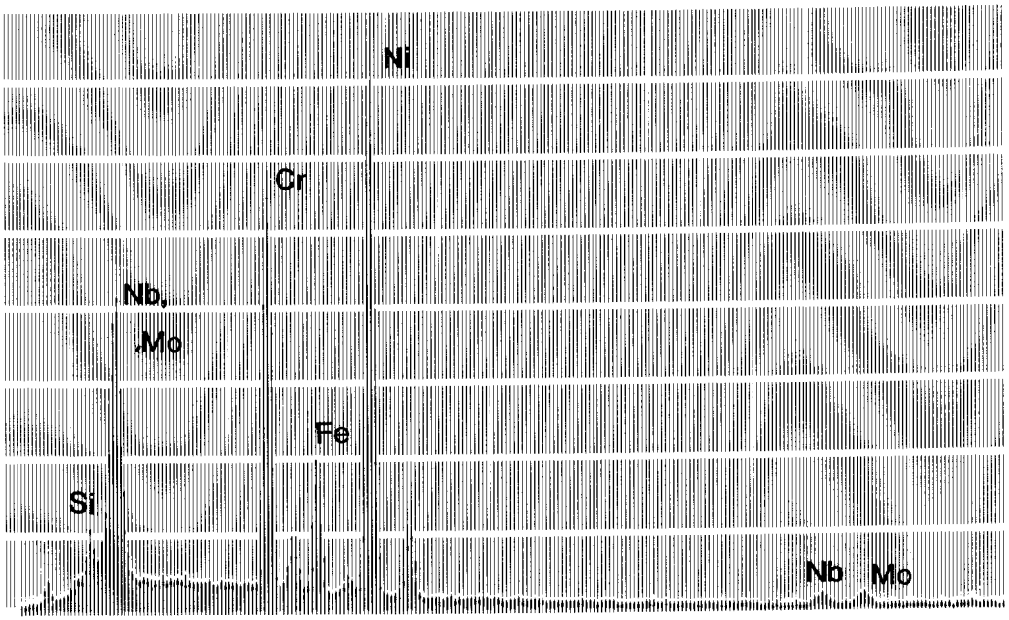

(A)

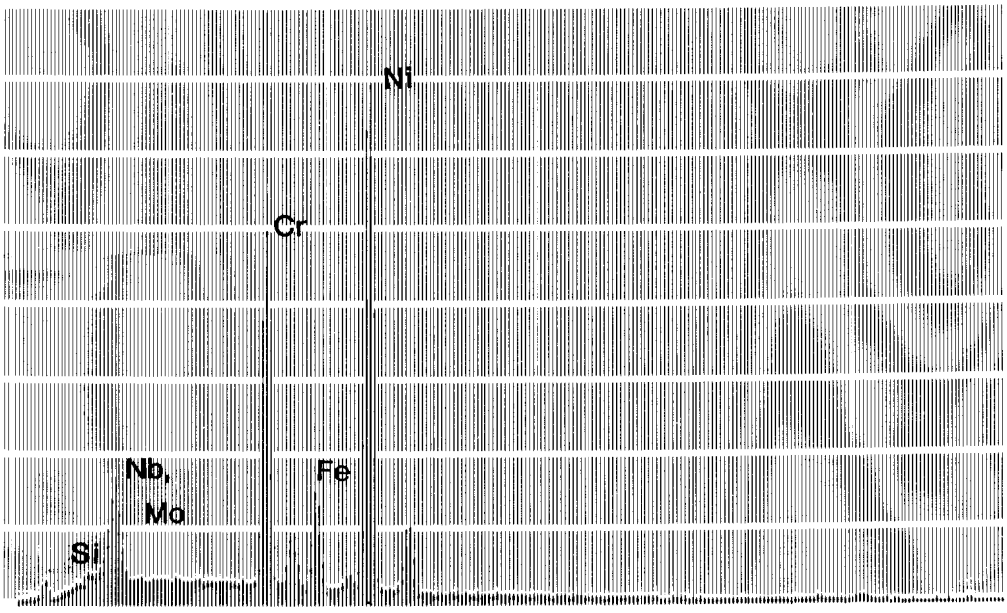

(B)

Fig. 8: EDXA Spectrum of (A) Particle and (B) Matrix In Laser Weldment.

The welding parameters and the calculated heat inputs for each process are shown in Table 2. The high heat input of approximately 132KJ/in^2 with the 350° F. interpass temperature used in this preliminary investigation of the PTA process would result in relatively slow cooling through the solidification range. Slow cooling would allow time for the rejection of the Si, Mo, and Nb into the interdendritic spaces resulting in a large volume of the terminal Laves phase and a greater chance for cracking to occur. A similar high heat input was used by Cieslack for GTAW welding of alloy 625 Plus in which he observed cracking (Ref. 2). The heat input in the GTAW process in this study was significantly less at 67 KJ/in^2 with an interpass temperature of 250° F. This heat input would result in more rapid cooling and less time available for segregation. Rapid cooling would promote a lower degree of segregation of the alloy constituents and the smaller particle size of the terminal phase. The faster cooling rate would also lead to a finer dendrite spacing (Ref. 6), resulting in a finer dispersion of the terminal phase. This demonstrates that the heat input is a more important factor in the cracking, than other weld process parameters. The laser process was conducted to produce the lowest heat input; see Table 2, just below that for the GTAW process. The degree of segregation; see Table 3, is similar for the two processes. There is a difference in the size and distribution of the terminal solidification phase; see Figs. 4 and 6. This suggests that, at these lower levels, the reduced heat input and faster cooling rate, had a greater effect on distribution of the terminal phase than on the degree of segregation leading to it.

The difference between the high heat input PTA welds, which cracked, and the lower heat input GTAW and laser welds which did not crack, is significant. No sign of cracking was observed in the GTAW process weldments and it is possible that higher heat inputs and deposition rates are possible before a cracking threshold is reached. Alternately, a lower heat input PTA process could be used to achieve higher deposition rates than the GTAW. Acceptable deposition rates were achieved for our application using parameters close to those listed for the GTAW process.

Conclusions

Alloy 625 is susceptible to cracking during welding due to the formation of Laves phase. Cracking can be avoided by reducing heat input during the welding process. Acceptable deposition rates were achieved at the reduced heat input.

Acknowledgements

The authors would like to acknowledge the following people for their expert assistance in the welding and preparation of the samples used in this investigation: G.M. Burcin, A.M. Delenne, V.J. Friscarella, T.A. Mullin and J.A. Rosepink.

References

1. Copson, H.R. and Economy, G. 1968. Effect of Some Environmental Conditions on Stress Corrosion Behavior of Ni-Cr-Fe Alloys in Pressurized Water. Corrosion 24 (3), No. 3: 55.

2. Cieslack, M.J., Headley, T.J., and Frank, R.B., 1989. The Welding of Custom Age 625 Plus Alloy. The Welding Journal 68 (12): 473-s to 482-s.

3. Ernst, S.C., Baeslack III, W.A., and Lippold, J.C., 1989. Weldability of High-Strength Low-Expansion Superalloys. The Welding Journal 68 (10): 418-s to 430-s.

4. Thomas Jr., R.D., 1984. HAZ Cracking in Thick Sections of Austenitic Stainless Steels - Part II. The Welding Journal 63 (12): 355-s to 368-s.

5. Cieslack, M.J., 1991. The Welding and Solidification Metallurgy of Alloy 625. The Welding Journal 70 (2): 49-s to 56-s.

6. Chalmers, B., 1967. Principles of Solidification. John Wiley and Sons, Inc., p. 120, New York.